Pergamon

Journal of Structural Geology, Vol. 19, Nos 3–4, pp. 243 to 248, 1997

0191-8141/97 $17.00 + 0.00

PII: S0191-8141(96)00092-2

Geometric analysis of hybrid fault-propagation/detachment folds

RANDALL MARRETT

Department of Geological Sciences, University of Texas at Austin, Austin, TX 78712-1101, U.S.A.

and

PETER A. BENTHAM

Exploration and Production Technology Group, Amoco Corporation, P.O. Box 3092, Houston, TX 77253-3092, U.S.A.

(*Received* 23 *January* 1996; *accepted in revised form* 8 *October* 1996)

Abstract—Fault-propagation folds and many detachment folds may be analyzed using a single geometric model. A modification of a previously published approach allows the interpreter to quantitatively predict thrust fault trajectory and displacement from the geometry of an associated fault-propagation/detachment anticline. Because geological and geophysical data typically constrain the mesoscopic and macroscopic forms of folds more completely and more accurately than they constrain faults, this technique offers a useful way to rapidly construct balanced structural cross-sections in detached fold–thrust systems. © 1997 Elsevier Science Ltd. All rights reserved.

INTRODUCTION

Fault-propagation and detachment folding are two mechanisms commonly employed to explain and quantitatively analyze fold development in contractional terrains. Geometric models that describe and generalize these fold styles are important tools for constructing geological cross-sections that balance (Dahlstrom, 1969; Laubscher, 1977; Suppe, 1983; Jamison, 1987). Field observations, map relationships, well-data and seismic reflection surveys commonly constrain the geometries, sizes and locations of folds in fold–thrust belts more tightly than they indicate the trajectories, displacements and locations of associated faults. As a result, the process of constructing a subsurface structural interpretation often involves inferring the characteristics of faults from the geometries of associated folds (Mitra, 1992).

The intent of this short paper is to further develop and illustrate the application of one particular published geometric model (Chester and Chester, 1990) that has significant utility for the prediction of subsurface fault characteristics when only folds may be confidently described. With the inclusion of an additional parameter describing the scale of a fold and reorganization of the equations that were presented in the original paper (Chester and Chester, 1990), it is possible to use surface fold observations to predict not only the dip and location of the associated blind thrust surface, but also the displacement on the fault surface required to generate the observed fold. These parameters provide important constraints for the generation of both prospect and regional-scale structural models in fold–thrust systems.

The fold model is based on the assumptions of plane strain, and conservation of both layer-parallel line length (except in the anticlinal forelimb) and cross-sectional area. It also employs parallel, kink-style folding and fold-hinges that migrate with respect to material points within the units being deformed (i.e. constant limb-dip folding of Epard and Groshong, 1995). The model addressed here, initially developed to describe fault-propagation folding alone, has two distinct advantages over those that preceded it (e.g. Suppe and Medwedeff, 1984, 1990; Suppe, 1985; Mitra, 1990). Firstly, the displacement gradient in the vicinity of the propagating fault-tip is not required to affect all layers that have been cut by the fault ramp. Secondly, the anticlinal backlimb of the fold that is generated is not required to dip parallel to the underlying fault ramp.

The second innovation implicitly generalizes both fault-propagation folds and a class of detachment folds into a single geometric model, although this apparently has not been appreciated previously. One can consider these 'detachment' folds to be developed above propagating fault ramps of very low dip. Consequently, the height of the associated fault ramp is typically less that the thickness of a stratigraphic unit on a regional-scale cross-section and the resulting geometries appear as detachment folds, namely anticlines in which neither the forelimb nor the backlimb parallel the associated fault ramp and which developed above the propagating tip of nearly bedding-parallel faults. The detachment fold model described by Dahlstrom (1990) may be considered an end-member of the model. The model described here, however, does not address detachment folds that require fold-limb rotation during development (e.g. Jamison, 1987). We illustrate the application of this model with two examples of well-exposed macroscopic folds from the Sierra Madre Oriental of northeastern and east-central

Mexico, both of which can be considered detachment folds.

MODEL GEOMETRY

For a detailed description of the model geometry employed by Chester and Chester (1990), the reader is referred to the original article. Most importantly, one should be aware of the key differences between the Chester and Chester (1990) model and those that preceded it. Namely, the anticlinal backlimb dip is independent of the dip of the associated fault ramp and the displacement gradient related to folding need not affect the entire hanging wall ramp, only a portion of it (Fig. 1). The fold initiation point, P, marks the location at which displacement begins to decrease and the fault tip point, T, occurs where displacement reaches zero. Fault displacement is assumed to change linearly between these two points.

In this analysis the fold parameters that must be known in order to characterize the dip of the associated fault surface are the backlimb dip measured relative to any regional inclination (2θ), the interlimb angle (γ), and the thickness-change ratio of layering within the forelimb of the fold (t_f/t). These parameters are related to the fault ramp dip relative to regional dip (α) by equation (4) of Chester and Chester (1990). Because this equation does not express geometric relationships for a single variable, the usefulness of the equation is basically limited to determining whether a set of input parameters are internally consistent with the model geometry or not. In order to use this relationship more predictively, a little trigonometry is necessary. Solving the equation (see Appendix) for the ramp dip (α) yields:

$$\alpha = \operatorname{acot}\left[-A - B + \sqrt{(A+B)^2 + 2A\cot(2\theta+\gamma) - \left(\frac{t_f}{t}\right)^2}\right] \quad (1)$$

where

$$A \equiv \tan\theta - \frac{1}{2}\left[\left(\frac{t_f}{t}\right)^2 + 1\right]\cot\gamma - \frac{t_f}{t}\csc\gamma$$

and

$$B \equiv \frac{1}{2}\left[\left(\frac{t_f}{t}\right)^2 - 1\right]\cot(2\theta+\gamma).$$

Importantly, equation (1) demonstrates the existence of a unique fault ramp dip corresponding to a locally balanced fault-propagation/detachment fold of a specific geometry. The relationship between ramp dip (α) and the angles defining the fold geometry is shown graphically in Fig. 2. The nomogram was calculated for the case where $t_f = t$, such that no layer thickness changes occur within the forelimb of the fold. Figure 2 clearly shows that ramp dip depends most sensitively on fold interlimb angle. For example, with a constant backlimb dip of 30°, increasing the fold interlimb angle from 30 to 90° increases the associated ramp dip by about 30°. Conversely, for a fixed interlimb angle, variations in the backlimb dip of a fold correspond to only minor changes in ramp dip. Notice that for tight anticlines ($0° \leq \gamma \leq 30°$), the ramp dip will always be very low ($\alpha \leq \sim 10°$) and the resulting geometry will essentially be that of a detachment fold. Such folds may vary from upright through highly vergent geometries with only minimal differences in ramp dip. In the extreme case of an isoclinal anticline, the ramp dip goes to zero and the resulting geometry is that of the detachment fold model of Dahlstrom (1990).

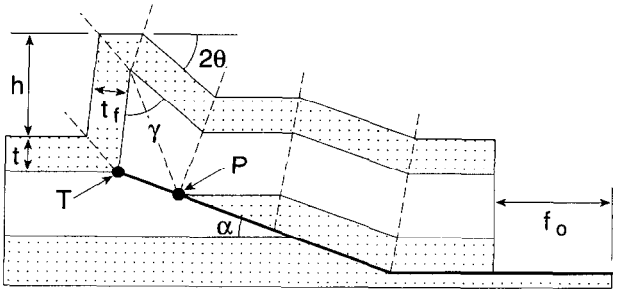

Fig. 1. Geometry of fault-propagation/detachment fold model employed in the analysis (modified after Chester and Chester, 1990).

Because the discussion above assumes $t_f = t$, the sensitivity of ramp dip to the forelimb thickness-change ratio cannot be appreciated. Figure 3 shows that tight interlimb angles (and consequently low ramp dips) produce only minor ramp angle sensitivity to forelimb thickness-change ratio. Open interlimb angles result in significant sensitivity to forelimb thickness-change ratio, particularly for anticlines with large backlimb dips. In general, thickening of the forelimb tends to decrease the calculated ramp angle and thinning of the forelimb tends to increase the ramp angle.

To more completely specify the fault surface for inclusion into a structural model or cross-section, the

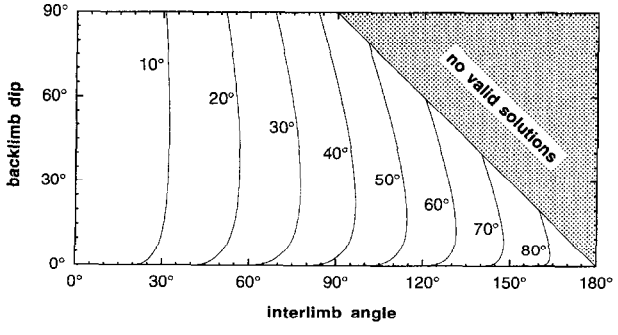

Fig. 2. Nomogram of ramp dip (α) as a function of changing backlimb dip (2θ) and interlimb angle (γ) assuming that $t_f/t = 1$. Curves follow the constant values of α indicated. Stippled area of the graph corresponds to the various combinations of input parameters that cannot result in a meaningful value of α. In this field, the sum of 2θ and γ is greater than 180°, and as such does not represent a sensible anticlinal geometry.

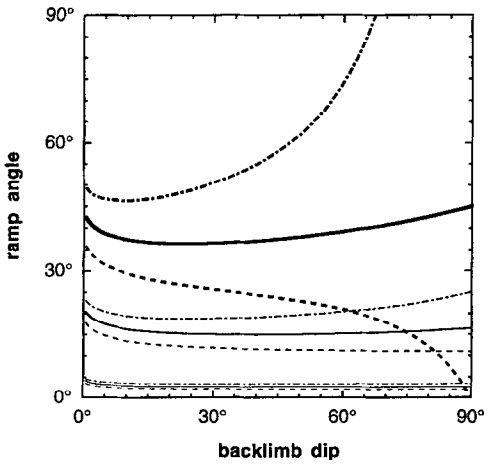

Fig. 3. Sensitivity of ramp dip (α) to forelimb thickness-change ratio (t_f/t) for a range of backlimb dips (2θ) and interlimb angles (γ). Thin curves correspond to $\gamma = 10°$; medium curves correspond to $\gamma = 45°$; bold curves correspond to $\gamma = 90°$. Continuous curves correspond to $t_f/t = 1$; dashed curves correspond to $t_f/t = 1.25$; dash-dotted curves correspond to $t_f/t = 0.8$.

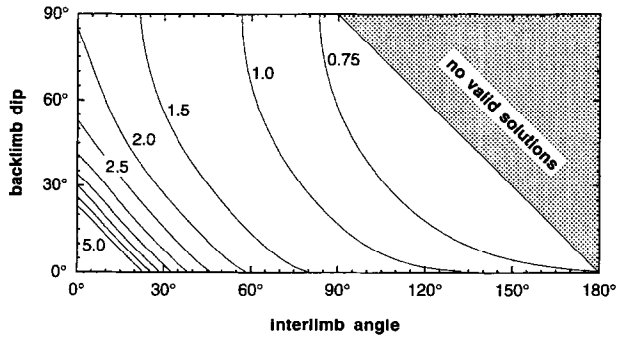

Fig. 4. Nomogram of normalized fault displacement (f_o/h) as a function of variations in backlimb dip (2θ) and interlimb angle (γ) assuming that $t_f/t = 1$. Curves follow the indicated values of normalized displacement, and may be multiplied by h for a specific anticline in order to calculate the true displacement, f_o. Stippled area of the graph corresponds to the various combinations of input parameters that cannot result in a meaningful fold geometry.

fault displacement associated with folding must be understood. In order to quantitatively predict fault displacement using the observed fold geometry it is necessary to define two additional parameters, namely, the structural relief of the anticline measured othogonal to regional (h) and the fault-parallel distance between the fault tip and the fold initiation point (TP). The distance TP and the displacement on the fault surface (f_o) may be calculated (see Appendix) using the following equations:

$$TP = hC \csc(2\theta + \gamma - \alpha) \tag{2}$$

and

$$f_0 = hC\left[\frac{t}{t_f}\csc\alpha - \csc(2\theta + \gamma - \alpha)\right] \tag{3}$$

where

$$C \equiv \frac{\csc(2\theta + \gamma)}{\frac{t}{t_f}\csc\gamma + \cot\gamma - \cot(2\theta + \gamma - \alpha)}.$$

Figures 4 and 5 show nomograms of fault displacement and TP distance, respectively, in terms of the fold interlimb angle and backlimb dip. As with the previous discussion, these solutions are generated for the case where no thickness change occurs within the forelimb of the fold ($t_f = t$). The fault displacement and TP distance values have been normalized to the structural relief of the anticline to remove the scale dependence of these calculations. It is clear that the normalized displacement and TP distance are sensitive to changes in both fold angles. For a given anticlinal structural relief, fault displacement increases with a decrease in backlimb dip and/or a decrease in interlimb angle. The TP distance systematically increases with increasing interlimb angle, but varies in a more complex fashion in terms of the backlimb dip. Figures 6 and 7 show that normalized fault displacement and TP distance, respectively, have only minor sensitivity to forelimb thickness-change ratio except for anticlines having both open interlimb angles and steep backlimb dips. Forelimb thickening increases both calculated displacement and TP distance, and forelimb thinning decreases both displacement and TP distance, with the exception of forelimb thinning of folds with open interlimb angles.

The final information needed to fully characterize the fault is its location. Recognizing that the Chester and Chester (1990) model geometry requires that the fault tip point, T, lies within the leading synclinal fold-hinge and that the fold initiation point, P, is located at the point where the anticlinal hinge intersects the fault, it is possible to construct the unique thrust-ramp that will satisfy the associated values of α and TP. Independent knowledge of the detachment level, or depth projection of the trailing synclinal fold-hinge, constrains the location of the ramp-

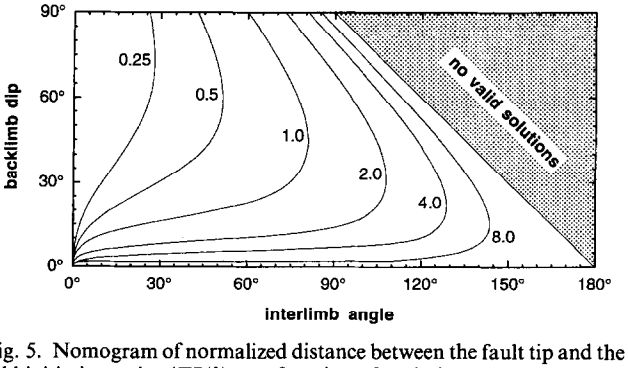

Fig. 5. Nomogram of normalized distance between the fault tip and the fold initiation point (TP/h) as a function of variations in backlimb dip (2θ) and interlimb angle (γ) assuming that $t_f/t = 1$. Curves follow the indicated values of normalized TP, and may be multiplied by h for a specific anticline in order to calculate the true TP. Stippled area of the graph corresponds to the various combinations of input parameters that cannot result in a meaningful fold geometry.

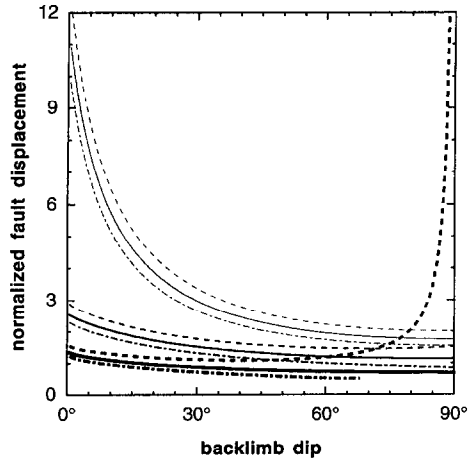

Fig. 6. Sensitivity of normalized fault displacement (f_o/h) to forelimb thickness-change ratio (t_f/t) for a range of backlimb dips (2θ) and interlimb angles (γ). Thin curves correspond to $\gamma = 10°$; medium curves correspond to $\gamma = 45°$; bold curves correspond to $\gamma = 90°$. Continuous curves correspond to $t_f/t = 1$; dashed curves correspond to $t_f/t = 1.25$; dash-dotted curves correspond to $t_f/t = 0.8$.

flat inflection in the fault trajectory. The distance from the ramp-flat inflection to the fold initiation point must be greater than or equal to the amount of displacement on the fault.

APPLICATIONS

The first example is drawn from a regional transect crossing numerous folds in the Monterrey Salient area of the Sierra Madre Oriental, northeastern Mexico. In this region, Laramide-age deformation affected a predominantly carbonate section of upper Jurassic through upper Cretaceous strata over a detachment within upper Jurassic gypsum/anhydrite evaporates of the Olvido Formation (e.g. Padilla y Sánchez, 1985). Evaporites crop out locally in the cores of anticlines, and represent the oldest exposed rocks in the Monterrey Salient. Surface maps and field studies were used to construct the geometry of a large anticline, which has a tight interlimb angle and verges towards the northeast (Fig. 8). The fold model parameters are a backlimb dip (2θ) of 49° and an interlimb angle (γ) of 25°. A structural relief above regional (h) of 3.0 km was estimated by projection of fold closure from out of the plane of the cross-section. Using equations (1)–(3) these data are consistent with a thrust ramp dip (α) of 7° and a TP distance of 0.8 km. A shortening of 5.1 km is predicted by the model. Using these calculations together with surface control of bedding dips, formational contacts and thicknesses, it is possible to complete the cross-section within the zone of detachment (Fig. 8).

The second example occurs to the south, in the eastern Sierra Madre Oriental fold-belt adjacent to the Veracruz Basin of east-central Mexico (Mossman and Viniegra, 1976). Here, a sequence of Cretaceous limestones are folded above a detachment (or series of shallowly-dipping thrust faults) within the Middle Cretaceous Orizaba Formation, which contains interbedded evaporates. A structural transect across one of these folds is shown in the upper portion of Fig. 9. Downward projection of surface dip control suggests that this fold verges towards the east, and has a steep to locally-overturned eastern limb. The primary fold parameters derived from detailed field work are a backlimb dip (2θ) of 67°, an interlimb angle (γ) of 19° and a structural relief above regional (h) of 1.7 km. These input data result in a predicted fault ramp dip of 5°, a TP distance of 0.29 km, and fault displacement of 2.7 km. This information was used to complete the cross-section and to project the thrust fault down-dip into its detachment (Fig. 9).

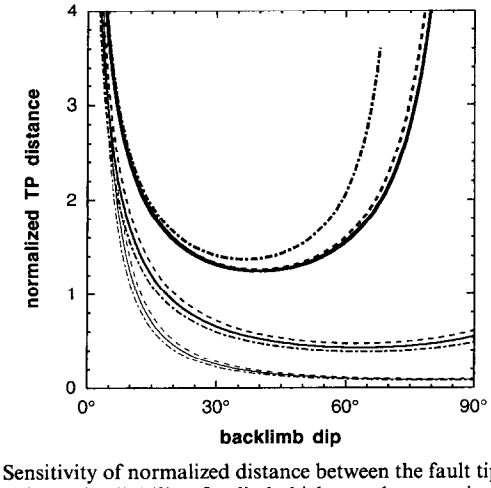

Fig. 7. Sensitivity of normalized distance between the fault tip and the fold initiation point (TP/h) to forelimb thickness-change ratio (t_f/t) for a range of backlimb dips (2θ) and interlimb angles (γ). Thin curves correspond to $\gamma = 10°$; medium curves correspond to $\gamma = 45°$; bold curves correspond to $\gamma = 90°$. Continuous curves correspond to $t_f/t = 1$; dashed curves correspond to $t_f/t = 1.25$; dash-dotted curves correspond to $t_f/t = 0.8$.

DISCUSSION AND CONCLUSIONS

The thrust trajectory, displacement and location of a fault can be uniquely determined from the form of an associated fault-propagation/detachment fold in a fold-thrust belt. While this model is able to rapidly predict a balanced fold-thrust relationship based on the present-day fold geometry, it does not claim to treat the kinematic development of such a system (Epard and Groshong, 1995; Homza and Wallace, 1995). The model employs constant limb-dip folding with migrating fold hinges that may not be kinematically consistent with other field observations. As such, the utility of this approach lies largely on its ability to use fold form to quantitatively predict associated faults at depth when little or no subsurface information is available.

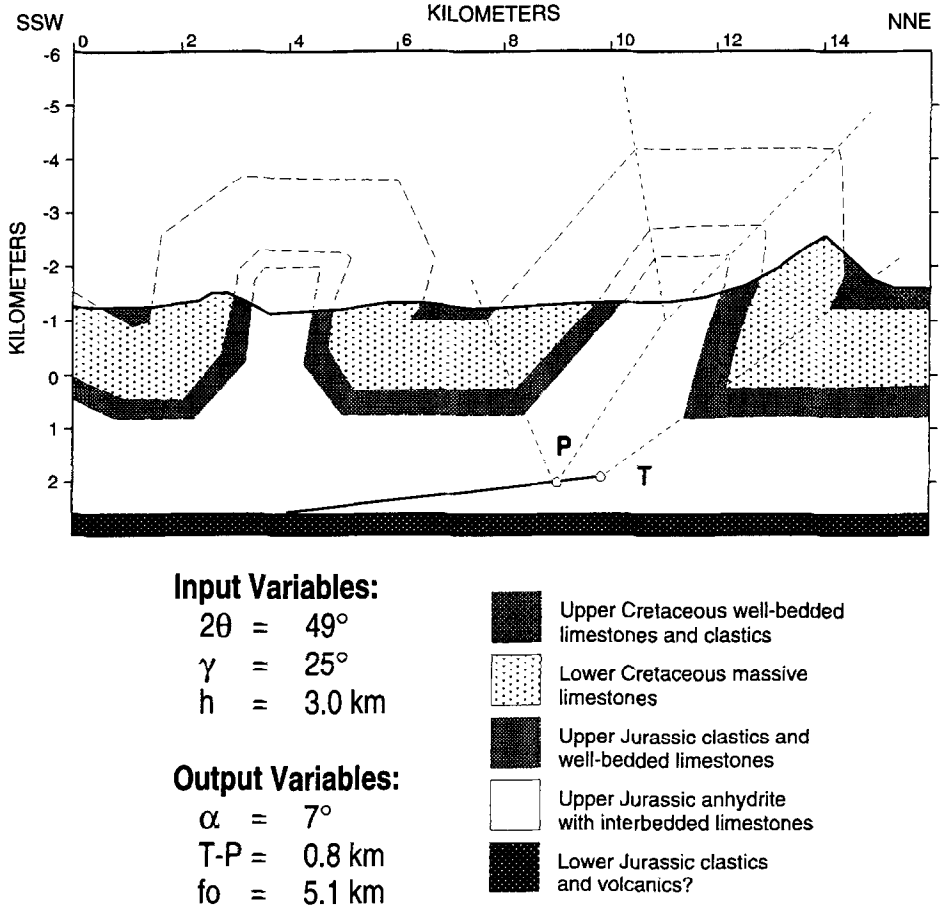

Fig. 8. Example application of the geometric model to a large surface anticline from northeastern Mexico. The section shown is part of a longer, regional-scale cross-section across the Sierra Madre Oriental.

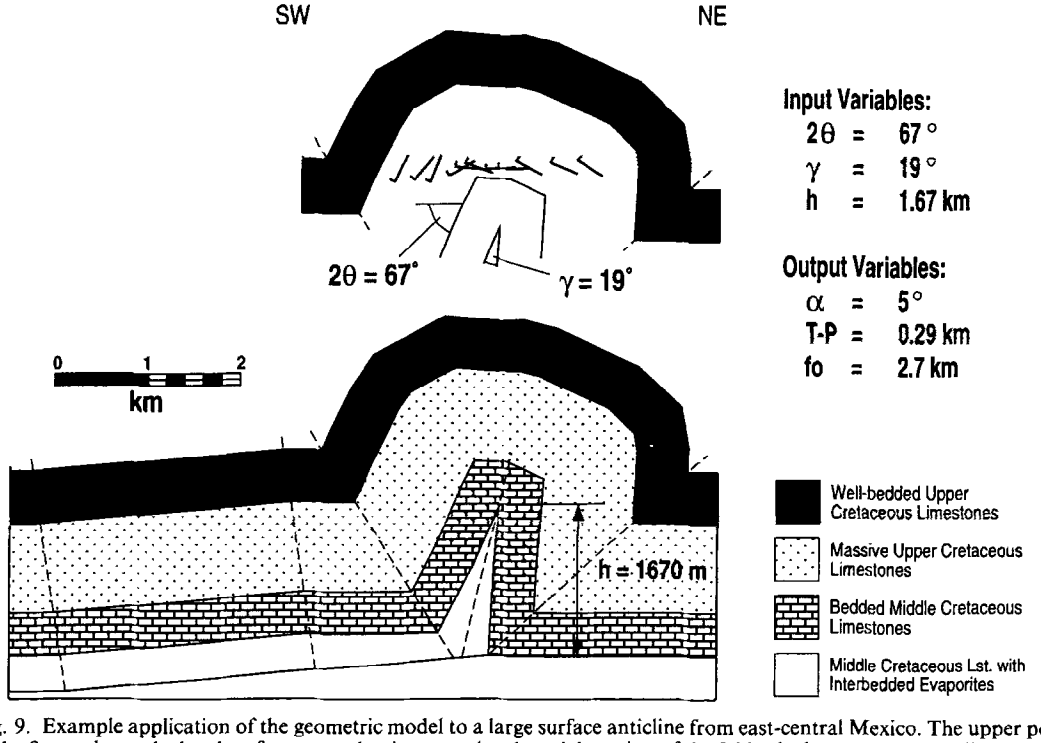

Fig. 9. Example application of the geometric model to a large surface anticline from east-central Mexico. The upper portion of the figure shows the local surface control as it constrains the axial portion of the fold. The lower part of the diagram shows part of a longer, regional cross-section across the fold of interest.

Acknowledgements—The authors would like to thank the management of Amoco Corporation for supporting the research and granting permission for the publication of portions of the work presented in this article. Fieldwork was supported during regional structural evaluations and performed in association with personnel of Amoco Mexico and Petroleos Mexicanos. Mario Aranda drew the original version of the fold from the Monterrey Salient. Reviews by Jamie Jamison and Mark Fischer were very helpful.

REFERENCES

Chester, J. S. and Chester, F. M. (1990) Fault-propagation folds above thrusts with constant dip. *Journal of Structural Geology* **12**, 903–910.

Dahlstrom, C. D. A. (1969) Balanced cross sections. *Canadian Journal of Earth Sciences* **6**, 743–757.

Dahlstrom, C. D. A. (1990) Geometric constraints derived from the law of conservation of volume and applied to evolutionary models for detachment folding. *Bulletin of the American Association of Petroleum Geologists* **74**, 336–344.

Epard, J.-L. and Groshong, R. H. (1995) Kinematic model of detachment folding including limb rotation, fixed hinges and layer parallel strain. *Tectonophysics* **247**, 85–103.

Homza, T. K. and Wallace, W. K. (1995) Geometric and kinematic models for detachment folds with fixed and variable detachment depths. *Journal of Structural Geology* **17**, 575–588.

Jamison, W. R. (1987) Geometric analysis of fold development in overthrust terrains. *Journal of Structural Geology* **9**, 207–219.

Laubscher, H. P. (1977) Fold development in the Jura. *Tectonophysics* **37**, 337–362.

Mitra, S. (1990) Fault-propagation folds: Geometry, kinematic evolution and hydrocarbon traps. *Bulletin of the American Association of Petroleum Geologists* **74**, 921–945.

Mitra, S. (1992) Balanced structural interpretations in fold and thrust belts. In *Structural Geology of Fold and Thrust Belts*, eds S. Mitra and G. W. Fisher, pp. 53–77. The Johns Hopkins University Press, Baltimore.

Mossman, R. W. and Viniegra, F. (1976) Complex fault structures in Veracruz Province of Mexico traps. *Bulletin of the American Association of Petroleum Geologists* **60**, 379–388.

Padilla y Sánchez, R. (1985) Las estructuras de la curvature de Monterrey, Estados de Coahuila, Nuevo León, Zacatecas y San Luis Potosí. *Revista Instituto de Géologia, Universidad Nacional Autónoma de México* **6**, 1–20.

Suppe, J. (1983) Geometry and kinematics of fault-bend folding. *American Journal of Science* **283**, 684–721.

Suppe, J. (1985). *Principles of Structural Geology*. Prentice-Hall, Englewood Cliffs, New Jersey.

Suppe, J. and Medwedeff, D. A. (1984). Fault-propagation folding. *Geological Society of America Abstracts with Programs* **16**, 670.

Suppe, J. and Medwedeff, D. A. (1990) Geometry and kinematics of fault-propagation folding. *Eclogae Geologicae Helveticae* **83**, 409–454.

APPENDIX

Equation (1) is derived from equation (4) of Chester and Chester (1990):

$$\cot\alpha + 2\tan\theta - \cot\gamma - 2\frac{t_f}{t}\csc\gamma + \left(\frac{t_f}{t}\right)^2[\cot(2\theta+\gamma-\alpha) - \cot\gamma] = 0. \tag{A1}$$

Substituting the trigonometric identity

$$\cot(2\theta+\gamma-\alpha) = \frac{\cot\alpha\cot(2\theta+\gamma)+1}{\cot\alpha - \cot(2\theta+\gamma)} \tag{A2}$$

into (A1), multiplying all terms of the resulting equation by the denominator of the identity, and simplifying we get:

$$\cot^2\alpha + \cot\alpha[2A+2B] + \left[\left(\frac{t_f}{t}\right)^2 - 2A\cot(2\theta+\gamma)\right] = 0, \tag{A3}$$

where A and B are as defined in the text. The quadratic solution to (A3) yields meaningful results only for the positive root, as used in equation (1).

Equation (2) derives from a restatement of equation (A16) of Chester and Chester (1990) as:

$$TP = t_f\csc(2\theta+\gamma-\alpha). \tag{A4}$$

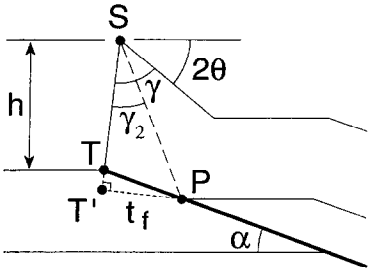

Fig. A1. Diagram defining the lengths and angles of triangles used to relate anticlinal structural relief to fault displacement and TP distance (modified after Chester and Chester, 1990).

In Fig. A1 we see that the structural relief of the anticline (h) can be expressed in terms of the layer-parallel length of the forelimb (ST):

$$h = ST\sin(2\theta+\gamma), \tag{A5}$$

and ST can in turn be written in terms of t_f:

$$ST = ST' - TT' = t_f[\cot\gamma_2 - \cot(2\theta+\gamma-\alpha)]. \tag{A6}$$

Substituting equation (A9) of Chester and Chester (1990),

$$\cot\gamma_2 = \frac{\frac{t}{t_f}+\cos\gamma}{\sin\gamma}, \tag{A7}$$

into (A6) yields:

$$ST = t_f\left[\frac{t}{t_f}\csc\gamma + \cot\gamma - \cot(2\theta+\gamma-\alpha)\right]. \tag{A8}$$

Finally, combining (A5) and (A8) yields $t_f = hC$, where C is as defined in the text, and substituting this result into (A4) yields equation (2).

Equation (3) derives from equation (A16) of Chester and Chester (1990), expressed in terms of fault displacement (f_o):

$$f_o = \frac{t}{\sin\alpha} - TP. \tag{A9}$$

Using (A4) from above:

$$t = \frac{t}{t_f}t_f = \frac{t}{t_f}\frac{TP}{\csc(2\theta+\gamma-\alpha)}. \tag{A10}$$

Substituting (A10) and equation (2) into (A9) yields equation (3).